

# Second Order Multigrid Methods for Elliptic Problems with Discontinuous Coefficients on an Arbitrary Interface

Armando Coco<sup>1</sup>, Giovanni Russo<sup>2</sup>

## 1 Introduction

Elliptic equations with discontinuous coefficients across a codimensional-one interface arise in several applications. Interface-fitted grid methods are difficult to use in the case of moving interfaces, because of the computationally expensive meshing procedures needed at each time step. In such cases an approach treating the interface as embedded in a Cartesian grid may be preferred. For the methods based on embedding the domain in a Cartesian grid, a detailed survey can be found in [6].

Multigrid technique is one of the most efficient strategy to solve a class of partial differential equations, using a hierarchy of discretizations. Several multigrid approaches exist in literature to treat the jumping coefficient problem in 2D when the interface is aligned with the Cartesian grid. We mention the method based on operator-dependent interpolation [2, 5], where the interpolation is carried out by exploiting the continuity of the flux instead of the gradient of the solution, and the method based on Galerkin Coarse Grid Operator [7]. Other relevant papers are [1, 10, 11].

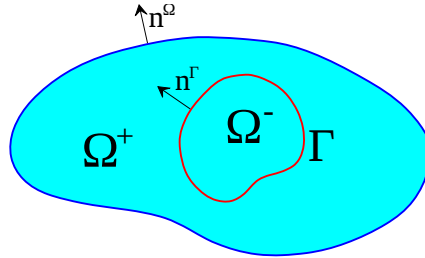
In this work, the method proposed in [4] to treat the discontinuous coefficient case in one dimensional problems is extended in higher dimensions. We obtain second-order accuracy in the solution and the gradient. A proper multigrid solver is described, following the technique used in [3] for continuous coefficients and mixed boundary conditions.

## 2 Model Problem

Let  $D = [-1, 1]^2$  be the computational domain and  $\Omega \subset D$  be a domain such that  $\partial\Omega \cap \partial D = \emptyset$ . Let us consider a partition  $\Omega = \Omega^- \cup \Omega^+$ , i.e.  $\Omega^+$  and  $\Omega^-$  are two non-empty domains such that  $\overset{\circ}{\Omega}^- \cap \overset{\circ}{\Omega}^+ = \emptyset$ . Let  $\Gamma$  be the *interface* separating the two subdomains, i.e.  $\Gamma = \partial\Omega^- \cap \partial\Omega^+$ , while the *boundary* is  $\partial\Omega$ . Consider the following Model Problem:

Model problem 1:

$$\left\{ \begin{array}{ll} -\nabla \cdot (\beta^\pm \nabla u^\pm) &= f^\pm \text{ in } \Omega^\pm \\ \llbracket u \rrbracket &= g_D \text{ on } \Gamma \\ \left[ \left[ \beta \frac{\partial u}{\partial n} \right] \right] &= g_N \text{ on } \Gamma \\ u &= g \text{ on } \partial\Omega \end{array} \right. \quad (1)$$



where  $\beta^-$  and  $\beta^+$  are positive functions. With  $\llbracket \cdot \rrbracket$  we denote the jump across the interface  $\Gamma$ . The domains and the interface are implicitly known by two level set functions  $\phi$  and  $\phi^\Gamma$  in such a way:

$$\begin{aligned} \Omega &= \{(x, y) : \phi(x, y) < 0\}, \quad \Omega^- = \{(x, y) : \phi^\Gamma(x, y) < 0 \text{ and } \phi(x, y) < 0\}, \\ \Omega^+ &= \{(x, y) : \phi^\Gamma(x, y) > 0 \text{ and } \phi(x, y) < 0\}, \quad \Gamma = \{(x, y) : \phi^\Gamma(x, y) = 0 \text{ and } \phi(x, y) < 0\}. \end{aligned} \quad (2)$$

<sup>1</sup> Dipartimento Scienze della Terra e Geoambientali, Università di Bari Aldo Moro, Bari, Italy

<sup>2</sup> Dipartimento di Matematica e Informatica, Università di Catania, Catania, Italy

Let us suppose that  $\phi$  and  $\phi^\Gamma$  are signed distance functions, i.e.  $|\nabla\phi| = 1$  (we can obtain the signed distance function by the level-set functions by reinitialization [8])

## 2.1 Notation

Let  $N \geq 1$  be an integer and  $h = 2/N$  the spatial step. Let  $D_h = \mathbf{j}h, \mathbf{j} = (j_1, \dots, j_d) \in \{-N, N\}^d$  be the discrete versions of  $D$ .  $D_h$  is the set of the *grid points*. Let  $\Omega_h^+ = \Omega^+ \cap D_h$  and  $\Omega_h^- = \Omega^- \cap D_h$  be the discrete versions of  $\Omega^+$  and  $\Omega^-$  respectively. Let  $\Gamma_h^{++}$  be the set of the *ghost points for  $\Omega^+$* , namely the grid points outside  $\Omega^+$  and belonging to some five-point stencil centered in a grid point inside  $\Omega^+$ , i.e.

$$(x, y) \in \Gamma_h^{++} \iff (x, y) \in D_h \setminus \Omega_h^+ \text{ and } \{(x \pm h, y), (x, y \pm h)\} \cap \Omega_h^+ \neq \emptyset.$$

Similarly we define  $\Gamma_h^{--}$  and  $\Gamma_h$  the set of the *ghost points for respectively  $\Omega^-$  and  $\Omega$* . Let us define  $\Gamma_h^- = \Gamma_h^{--} \setminus \Gamma_h$  and  $\Gamma_h^+ = \Gamma_h^{++} \setminus \Gamma_h$ . We call  $N_i^+ = |\Omega_h^+|$ ,  $N_g^+ = |\Gamma_h^+|$ ,  $N_i^- = |\Omega_h^-|$ ,  $N_g^- = |\Gamma_h^-|$ ,  $N_g = |\Gamma_h|$ ,  $N_i^{++} = |\Gamma_h^{++}|$ ,  $N_i^{--} = |\Gamma_h^{--}|$ .

## 3 Discretization of the problem

The final linear system coming from the discretization of the problem will consist in a  $\tilde{N} \times \tilde{N}$  linear system, where  $\tilde{N} = N_i^+ + N_g^+ + N_i^- + N_g^- + N_g$ . The  $N_i^-$  equations coming from the grid points of  $\Omega_h^-$  are obtained discretizing the first Eq. of (1) by usual central differences:

$$\beta_{i+1/2,j}^- (u_{i,j}^- - u_{i+1,j}^-) + \beta_{i-1/2,j}^- (u_{i,j}^- - u_{i-1,j}^-) + \beta_{i,j+1/2}^- (u_{i,j}^- - u_{i,j+1}^-) + \beta_{i,j-1/2}^- (u_{i,j}^- - u_{i,j-1}^-) = f_{i,j}^- h^2 \quad (3)$$

where  $\beta_{i\pm 1/2,j}^- = (\beta_{i,j}^- + \beta_{i\pm 1,j}^-)/2$ ,  $\beta_{i,j\pm 1/2}^- = (\beta_{i,j}^- + \beta_{i,j\pm 1}^-)/2$ . Similarly, we write an equation for each grid point of  $\Omega_h^+$ . Therefore, to close the linear system, we must write an equation for each ghost point  $G \in \Gamma_h \cup \Gamma_h^+ \cup \Gamma_h^-$ .

### 3.1 Discretization of the boundary conditions

Let  $G \in \Gamma_h$ . Then, we discretize the boundary condition on  $\Omega$ , i.e. the fourth equation of (1). We compute the outward unit normal in  $G$ , that is  $\mathbf{n}_G = (n_G^x, n_G^y) = \nabla\phi$ , using a second-order accurate discretization for  $\nabla\phi$ , such as central difference in  $G$ . Now we can compute the closest boundary point to  $G$ , that we call  $B$ , by the signed distance function:

$$B = G - \phi(G)\mathbf{n}_G. \quad (4)$$

Therefore, the equation of the linear system for the ghost point  $G$  is:

$$\tilde{u}(B) = g(B) \quad (5)$$

where  $\tilde{u}$  is the biquadratic interpolant of  $u$  on a suitable upwind nine-point stencil contained in  $\Omega_h \cup \Gamma_h$ . We choose the upwind nine-point stencil in the following manner (see Fig. 1 for the case  $n_x, n_y > 0$ , the other cases are analogous). If  $|x_B - x_G| < |y_B - y_G|$  (as in Figs. 1 and 2), the nine-point stencil will be composed by three points of the column  $i$ , three points of the column  $i - 1$ , three points of the column  $i - 2$ ; while if  $|x_B - x_G| \geq |y_B - y_G|$  it will be composed by three points of the row  $j$ , three points of the row  $j - 1$ , three points of the row  $j - 2$ . We prefer when possible the  $3 \times 3$  squared stencil.

If it is not possible to build the nine-point stencil, we revert to a more robust (less accurate) three-point stencil (Fig. 2):  $(i, j)h$ ,  $(i - 1, j)h$ ,  $(i, j - 1)h$ . Note that these three points belong to  $\Omega_h \cup \Gamma_h$ , since  $B \equiv (i, j)h \in \Omega_h$ .

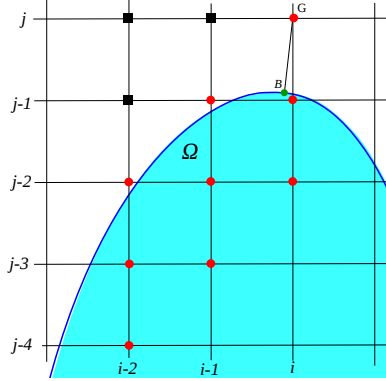


Fig. 1: The squared grid points do not belong to  $\Omega_h \cup \Gamma_h$ , thus they must be excluded from the nine-point stencil. The circled grid points are the modified nine-point stencil for the ghost point  $G$ .

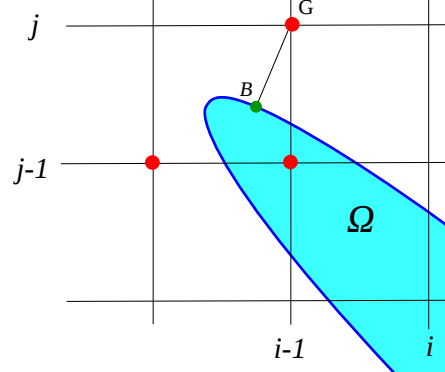


Fig. 2: Reduction of the nine-point stencil to a three-point stencil for the ghost point  $G$ .

### 3.2 Discretization of the interface conditions

If  $G \in \Gamma_h^- \cup \Gamma_h^+$  we discretize the interface conditions (second and third equations of (1)). We compute an approximation of the unit normal vector to  $\Gamma$  in  $G$  pointing from  $\Omega^-$  to  $\Omega^+$ , that is  $\mathbf{n}_G^\Gamma = (\nabla \phi^\Gamma)|_G$ , using a second order accurate discretization, such as central differences in  $G$ . Now we can compute the closest interface point to  $G$ , that we call  $I$ , as:

$$I = G - \mathbf{n}_G \cdot \phi(G). \quad (6)$$

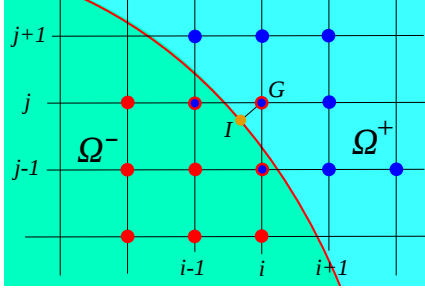


Fig. 3: In this figure  $G \in \Gamma_h^-$ . The blue nine-point stencil is contained in  $\Omega_h^+ \cup \Gamma_h^+$  and serves for interpolating  $\tilde{u}^+$ ; the red nine-point stencil is contained in  $\Omega_h^- \cup \Gamma_h^-$  and serves for interpolating  $\tilde{u}^-$ .

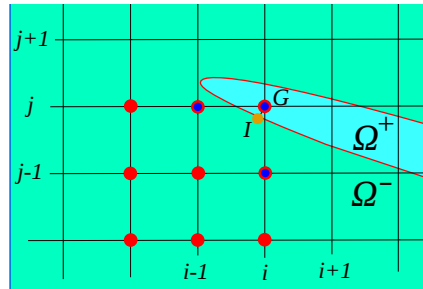


Fig. 4: In this figure  $G \in \Gamma_h^-$ . The nine-point stencil contained in  $\Omega_h^+ \cup \Gamma_h^+$  serving to interpolate  $\tilde{u}^+$  has been reduced to the blue three-point stencil.

The equation of the linear system for the ghost point  $G$  is obtained discretizing one of the jump conditions (second and third equation of (1)): more precisely, if  $G \in \Gamma_h^-$  we use one of the two jump conditions, while if  $G \in \Gamma_h^+$  we use the other jump condition. Which jump condition has to be used in each case constitutes a choice, that can be based, for example, on the condition number of the resulting linear system. Let us suppose we want to discretize the equation for the ghost point  $G \in \Gamma^-$  and that  $\beta^- < \beta^+$ . If we discretize the jump in the flux (third equation of (1)) to

construct the equation of the linear system, then the diagonal entry is multiplied by  $\beta^-$ , while some of the off-diagonal entries are multiplied by  $\beta^+ > \beta^-$ , leading to ill-conditioned system.

Therefore:

- if  $\{G \in \Gamma_h^+ \text{ and } \beta^+(I) < \beta^-(I)\}$  or  $\{G \in \Gamma_h^- \text{ and } \beta^+(I) > \beta^-(I)\}$ , then the equation for the ghost point  $G$  is obtained from  $\llbracket u \rrbracket(I) = g_D(I)$ :

$$\tilde{u}_h^+(I) - \tilde{u}_h^-(I) = g_D(I) \quad (7)$$

- otherwise, it is obtained from  $\left\llbracket \beta \frac{\partial u}{\partial n} \right\rrbracket(I) = g_N(I)$ :

$$\left( \beta^+ \nabla \tilde{u}_h^+ - \beta^- \nabla \tilde{u}_h^- \right) \Big|_I \cdot \left( \frac{\nabla \tilde{\phi}_h}{|\nabla \tilde{\phi}_h|} \right) \Big|_I = g_N(I) \quad (8)$$

where  $\tilde{u}_h^+$  (resp.  $\tilde{u}_h^-$ ) is the biquadratic interpolant of  $u_h^+$  (resp.  $u_h^-$ ) in a suitable nine-point stencil contained in  $\Omega_h^+ \cup \Gamma_h^{++}$  (resp.  $\Omega_h^- \cup \Gamma_h^{--}$ ), and  $\tilde{\phi}_h$  is the biquadratic interpolant of  $\phi$  in a nine-point stencil surrounding  $I$ . What is left is the choice of the nine-point stencils contained in  $\Omega_h^- \cup \Gamma_h^{--}$  and  $\Omega_h^+ \cup \Gamma_h^{++}$ . Let us suppose that  $G \in \Gamma_h^-$  (the case  $G \in \Gamma_h^+$  is treated similarly). The nine-point stencil contained in  $\Omega_h^- \cup \Gamma_h^{--}$  is chosen in upwind direction, as described in Sec. 3.1. The nine-point stencil contained in  $\Omega_h^+ \cup \Gamma_h^{++}$  will be set as follows: if  $|x_G - x_I| \geq |y_G - y_I|$  (as in Figs. 3 and 4) it will be composed by three points of the row  $j - 1$ , three points of the row  $j$ , three points of the row  $j + 1$ ; while if  $|x_G - x_I| < |y_G - y_I|$  it will be composed by three points of the column  $i - 1$ , three points of the column  $i$ , three points of the column  $i + 1$ .

If it is not possible to build the nine-point stencil, we revert to a more robust (less accurate) three-point stencil (Fig. 4):  $(i, j)h$ ,  $(i - 1, j)h$ ,  $(i, j - 1)h$ . Note that these three points belong to  $\Omega_h^+ \cup \Gamma_h^{++}$ , since  $G \equiv (i, j)h \in \Omega_h^+$ . If  $G \in \Gamma_h^-$  the procedure is the same, provided to interchange the subscripts  $+$  and  $-$ .

## 4 Multigrid approach

### 4.1 Relaxation scheme

Let us denote by  $A\mathbf{u} = \mathbf{f}$  the linear system obtained in Sec. 3, where  $A = (a_{k,l})_{k,l=1,\dots,\tilde{N}} \in \mathbb{R}^{\tilde{N} \times \tilde{N}}$ ,  $\mathbf{u}, \mathbf{f} \in \mathbb{R}^{\tilde{N}}$ , with  $\tilde{N} = N_i^+ + N_g^+ + N_i^- + N_g^- + N_g$ . The relaxation scheme of the multigrid is obtained by the following Richardson iteration:

$$\mathbf{u}^{(m+1)} = \mathbf{u}^{(m)} + P^{-1}(\mathbf{f} - A\mathbf{u}) \quad (9)$$

with a diagonal preconditioner  $P$ . Let us call  $\tilde{D} = \text{diag}(d_k)_{k=1,\dots,\tilde{N}}$  a diagonal matrix such that the diagonal entries satisfy the following two properties:

$$|d_k| \geq \max_{l=1,\dots,\tilde{N}} |a_{k,l}|, \quad d_k \cdot a_{k,k} > 0. \quad (10)$$

If  $k$  refers to an inner equation, we choose  $d_k = \max_{l=1,\dots,\tilde{N}} |a_{k,l}|$  (see (3)), else if  $k$  refers to the boundary condition (see (5)) or the jump condition on the solution (see (7)) we choose  $|d_k| = 1$ , else if  $k$  refers to the jump condition on the flux (see (8)) we choose  $|d_k| = 3/2\sqrt{2} \max\{\beta^-, \beta^+\}$ . If we choose  $P = \tilde{D}$ , we observed numerically that the iteration scheme (9) is convergent. Furthermore, such iteration scheme is Jacobi-like for the inner equations, since  $d_k = |a_{k,k}|$ . Therefore, it is a suitable building-block for the multigrid solver. However, since we want to use a good smoother, we must use the weighted-Jacobi scheme or the Gauss-Seidel scheme. We switch to the Gauss-Seidel version of the scheme, i.e. we choose  $P = \tilde{D} + E$ , where  $E$  is the lower triangular part of  $A$ .

### 4.1.1 Smoothing property

The smoothing property of the Gauss-Seidel scheme depends on the ordering chosen for the variables. It is well known (see [9]) that the Red-Black Gauss-Seidel (RB-GS) scheme is a better smoother with respect to the Lexicographic Gauss-Seidel (LEX-GS) scheme, but, for simplicity, we just study the smoothing properties of the GS-LEX scheme, and we compare the convergence factor with the predicted one by the Local Fourier Analysis (see [9] for more details) for LEX-GS scheme. In order to avoid that the boundary effects degrade the convergence factor, we add some extra-relaxations (on each grid level and for each relaxation) on two suitable layers surrounding respectively the interface and the boundary, that is, chosen two parameters  $\lambda$  and  $\delta$ , we add  $\lambda$  extra-relaxations on the following two sets:

$$\Omega_h^{(\delta)} = \{P \in \Omega_h \text{ such that } -\phi(P) < \delta\}, \quad \Omega_h^{\pm(\delta)} = \{P \in \Omega_h^{\pm} \text{ such that } -\phi^{\Gamma}(P) < \delta\}.$$

We experienced that in this case a good choice of the parameters  $\lambda$  and  $\delta$  is  $\lambda = 5, \delta = 5h$ .

## 4.2 Extension operator

Let us consider the whole domain  $\Omega$  (the argument can be easily repeated with the two subdomains  $\Omega^-$  and  $\Omega^+$ ). Such a domain is defined by a level-set function  $\phi$  and it defines a set of inner grid points  $\Omega_h$  and a set of ghost points  $\Gamma_h$ . Let us suppose we know a grid function  $\omega_h$  defined in  $\Gamma_h$  and we want to extend such a function in all the domain  $D_h - \Omega_h$ . The extended function  $\omega_h^{ext}$  can be obtained extrapolating  $\omega_h$  constant along the normal direction to  $\partial\Omega$ , i.e. solving the transport equation  $\frac{\partial\omega}{\partial\tau} + \nabla\omega \cdot \mathbf{n} = 0$  in a few steps of a fictitious time  $\tau$ , where  $\omega = \omega_h$  in  $\Gamma_h$ , and  $\mathbf{n} \equiv (n_x, n_y) = \nabla\phi/|\nabla\phi|$  is the unit normal vector to the level-set. We can resume the extension process by an extension operator  $\omega_h^{ext} = \mathcal{E}[\Gamma_h; \phi_h](\omega_h)$ .

## 4.3 Transfer (restriction and interpolation) operators

We want to define a suitable restriction operator  $\mathcal{I}_{2h}^h$ . We perform the usual full-weighting restriction away from the boundary/interface. When we are close to the boundary/interface, we modify the restriction operator for inner equations in such a way we use only values coming from the same side of the boundary/interface, since the values from the other sides refer to a different operator, whether the value of the other side is considered as an inner point of the other subdomain (in which case we have a discontinuity of the operator) or it is considered as a ghost point (in which case the operator refers to the boundary/interface condition, that scales with a different power of  $h$ ). The modified restriction operator is represented in Fig. 5.

The restriction of the boundary/interface conditions is performed similarly, provided we extend the defect of the boundary/interface conditions away from the boundary/interface and then perform the same restriction procedure, using only the values coming from the same side of the boundary/interface. The procedure will be described in details in Sec. 4.4.

Since the interpolation operator acts on the error, which is supposed to be continuous across the boundary/interface, we use the standard linear interpolation operator.

## 4.4 Two-Grid Correction scheme

In order to describe the multigrid technique, we just describe the TGCS (Two-Grid Correction Scheme), since any other basic multigrid algorithm (such as  $V$ -cycle,  $W$ -cycle, Full Multigrid, and so on) can be easily derived from it (see [9] for more details). The TGCS consists into the following algorithm:

- Relax  $\nu_1$  times on the grid with spatial step  $h$ .

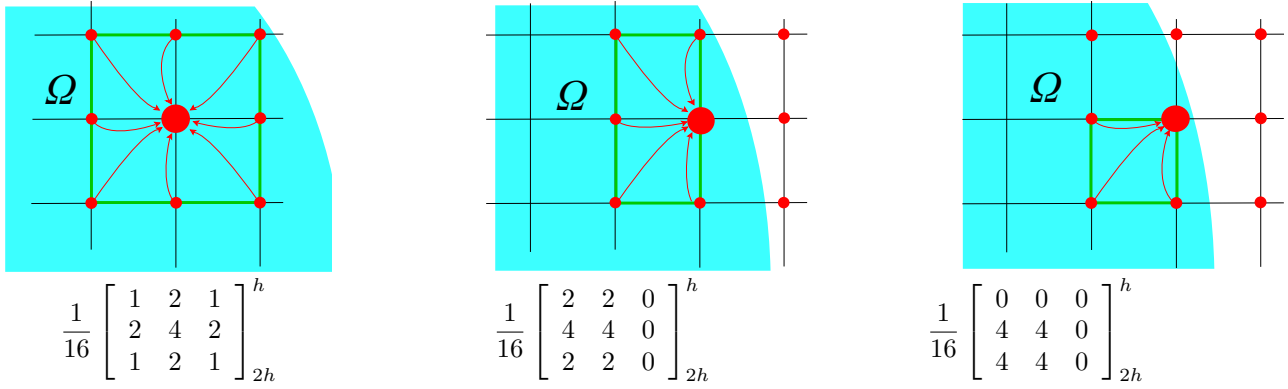


Fig. 5: Upper, the nine points of  $\mathcal{N}(x, y)$  and the green boundary of the rectangle  $\mathcal{T}$ . The bold red point is on the coarser and finer grids, while the little red points are on the finer grid. The arrows represent the action of the restriction operators. Below, the respective stencil to be used.

- Compute the defects:  $\mathbf{r}_h^{\Omega^-} = \mathbf{r}_h|_{\Omega_h^-}$ ,  $\mathbf{r}_h^{\Omega^+} = \mathbf{r}_h|_{\Omega_h^+}$ ,  $\mathbf{r}_h^{\Gamma^-} = \mathbf{r}_h|_{\Gamma_h^-}$ ,  $\mathbf{r}_h^{\Gamma^+} = \mathbf{r}_h|_{\Gamma_h^+}$ ,  $\mathbf{r}_h^{\Gamma} = \mathbf{r}_h|_{\Gamma_h}$ , where  $\mathbf{r}_h = \mathbf{f} - \mathbf{A}\mathbf{u}$ .
- Extend the defects  $\mathbf{r}_h^{\Gamma^-}$ ,  $\mathbf{r}_h^{\Gamma^+}$  and  $\mathbf{r}_h^{\Gamma}$ , using the extension operator defined in (4.2):

$$\mathbf{r}_h^{\Gamma^-, ext} = \mathcal{E}[\Gamma_h^-; -\phi_h](\mathbf{r}_h^{\Gamma^-}), \quad \mathbf{r}_h^{\Gamma^+, ext} = \mathcal{E}[\Gamma_h^+; \phi_h](\mathbf{r}_h^{\Gamma^+}), \quad \mathbf{r}_h^{\Gamma, ext} = \mathcal{E}[\Gamma_h; \phi_h](\mathbf{r}_h^{\Gamma}).$$

- Transfer these defects to a coarser grid with spatial step  $2h$  by the *restriction operator* defined in Sec. 4.3:

$$\mathbf{r}_{2h}^{\Omega^-} = I_{2h}^h(\mathbf{r}_h^{\Omega^-}), \quad \mathbf{r}_{2h}^{\Omega^+} = I_{2h}^h(\mathbf{r}_h^{\Omega^+}), \quad \mathbf{r}_{2h}^{\Gamma^-} = I_{2h}^h(\mathbf{r}_h^{\Gamma^-, ext}), \quad \mathbf{r}_{2h}^{\Gamma^+} = I_{2h}^h(\mathbf{r}_h^{\Gamma^+, ext}), \quad \mathbf{r}_{2h}^{\Gamma} = I_{2h}^h(\mathbf{r}_h^{\Gamma, ext}).$$

- Solve exactly the residual problem in the coarser grid.
- Transfer the error to the finer grid by the interpolation operator:  $\mathbf{e}_h = I_h^{2h}(\mathbf{e}_{2h})$ .
- Correct the fine-grid approximation  $\mathbf{u}_h := \mathbf{u}_h + \mathbf{e}_h$ .
- Relax  $\nu_2$  times on the grid with spatial step  $h$ .

## 5 Numerical tests

### 5.1 Example 1: circular domains

Let us consider the following data:

$$\begin{aligned} \phi^\Gamma(x, y) &= \sqrt{(x - x_0)^2 + (y - y_0)^2} - R_1, & \phi(x, y) &= \sqrt{(x - x_0)^2 + (y - y_0)^2} - R_2, \\ u^- &= \sin(4\pi x) \cos(6\pi y), & u^+ &= \cos(2\pi x) \sin(3\pi y), \\ \beta^- &= 10^6 + 10^5 \sin(\pi x) \cos(3\pi y), & \beta^+ &= 1 + 0.5 \sin(2\pi x) \cos(4\pi y) \end{aligned} \tag{11}$$

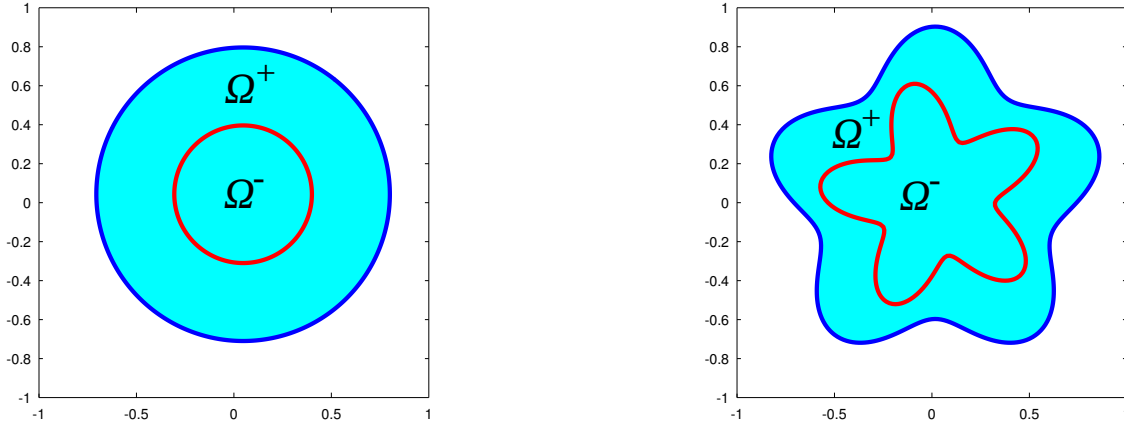


Fig. 6: Domains  $\Omega^-$  and  $\Omega^+$  of the Example 5.1 (left) and of the Example 5.2 (right).

or

$$\beta^- = 1 + 0.5 \sin(2\pi x) \cos(4\pi y), \quad \beta^+ = 10^6 + 10^5 \sin(\pi x) \cos(3\pi y). \quad (12)$$

We choose  $x_0 = \sqrt{2}/30$ ,  $y_0 = \sqrt{3}/40$ ,  $R_1 = 0.353$  and  $R_2 = 0.753$ . The domain is represented in Fig. 6 (left side). We performed one test with (11) and one test with (12). We list in Tables 1 and 2 the errors of the solution and its gradient in the  $L^1$  and  $L^\infty$  norms, while Fig. 7 shows the related bestfit lines. The error presented in Table 1 (and also in Table 3) is quite large. This phenomenon, which is physiological for this model, can be explained studying the residual equation for the discretization error and it is not imputable to the discretization scheme. Such analysis will be presented in a forthcoming paper.

Tab. 1: Example 5.1. Accuracy order in the solution and in the gradient for the case (11).

| $N^2$   | $L^1$ error of $u$ | order | $L^\infty$ error of $u$ | order | $L^1$ error of $ \nabla u $ | order | $L^\infty$ error of $ \nabla u $ | order |
|---------|--------------------|-------|-------------------------|-------|-----------------------------|-------|----------------------------------|-------|
| $32^2$  | $8.34 \cdot 10^3$  | -     | $7.70 \cdot 10^4$       | -     | $1.46 \cdot 10^5$           | -     | $3.90 \cdot 10^5$                | -     |
| $64^2$  | $2.07 \cdot 10^3$  | 2.01  | $1.85 \cdot 10^4$       | 2.06  | $3.49 \cdot 10^4$           | 2.06  | $1.06 \cdot 10^5$                | 1.88  |
| $128^2$ | $5.79 \cdot 10^2$  | 1.84  | $5.10 \cdot 10^3$       | 1.86  | $9.56 \cdot 10^3$           | 1.87  | $2.96 \cdot 10^4$                | 1.84  |
| $256^2$ | $1.46 \cdot 10^2$  | 1.99  | $1.28 \cdot 10^3$       | 2.00  | $2.39 \cdot 10^3$           | 2.00  | $7.45 \cdot 10^3$                | 1.99  |

Tab. 2: Example 5.1. Accuracy order in the solution and in the gradient for the case (12).

| $N^2$   | $L^1$ error of $u$   | order | $L^\infty$ error of $u$ | order | $L^1$ error of $ \nabla u $ | order | $L^\infty$ error of $ \nabla u $ | order |
|---------|----------------------|-------|-------------------------|-------|-----------------------------|-------|----------------------------------|-------|
| $32^2$  | $4.40 \cdot 10^{-3}$ | -     | $1.22 \cdot 10^{-1}$    | -     | $3.93 \cdot 10^{-1}$        | -     | $3.52 \cdot 10^0$                | -     |
| $64^2$  | $1.02 \cdot 10^{-3}$ | 2.11  | $2.93 \cdot 10^{-2}$    | 2.06  | $9.95 \cdot 10^{-2}$        | 1.98  | $9.71 \cdot 10^{-1}$             | 1.86  |
| $128^2$ | $3.29 \cdot 10^{-4}$ | 1.64  | $7.61 \cdot 10^{-3}$    | 1.95  | $2.63 \cdot 10^{-2}$        | 1.92  | $2.80 \cdot 10^{-1}$             | 1.80  |
| $256^2$ | $8.24 \cdot 10^{-5}$ | 2.00  | $2.14 \cdot 10^{-3}$    | 1.83  | $6.60 \cdot 10^{-3}$        | 1.99  | $7.32 \cdot 10^{-2}$             | 1.93  |

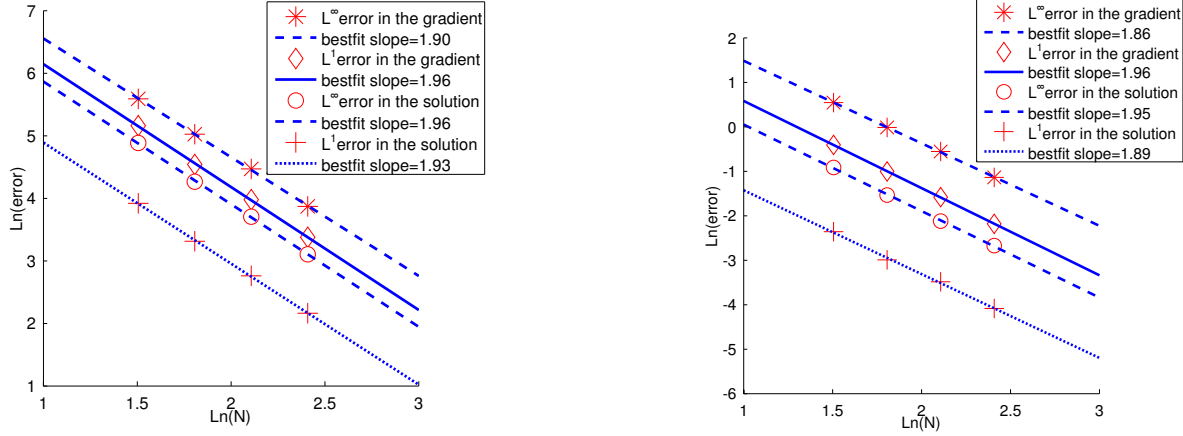


Fig. 7: Example 5.1. Bestfit lines of the errors in the solution and in the gradient (Tables 1 and 2) in both the  $L^1$  and  $L^\infty$  norms. Left:  $\beta^-$  and  $\beta^+$  are given by (11); Right:  $\beta^-$  and  $\beta^+$  are given by (12).

## 5.2 Example 2: flower-shaped domains

Let us consider the general flower-shaped interface with parametric equations:

$$X(\vartheta) = r(\vartheta) \cos(\vartheta) + x_0,$$

$$Y(\vartheta) = r(\vartheta) \sin(\vartheta) + y_0,$$

with  $\vartheta \in [0, 2\pi]$  and  $r(\vartheta) = r_0 + r_1 \sin(\omega\vartheta)$ . Let us consider  $\omega = 5$ . The level-set representation of this interface is:

$$flower(r_0, r_1, x_0, y_0; x, y) = r - r_0 - r_1 \frac{(y - y_0)^5 + 5(x - x_0)^4(y - y_0) - 10(x - x_0)^2(y - y_0)^3}{r^5}.$$

where  $r = \sqrt{(x - x_0)^2 + (y - y_0)^2}$ . Let us choose the following data:

$$\phi^\Gamma(x, y) = flower(0.45, 1/7, 0.01\sqrt{3}, 0.02\sqrt{2}; x, y), \quad \phi(x, y) = flower(0.75, 1/8, 0.01\sqrt{3}, 0.02\sqrt{2}; x, y),$$

$$u^- = \sin(4\pi x) \cos(6\pi y), \quad u^+ = \cos(2\pi x) \sin(3\pi y),$$

$$\beta^- = 10^6 + 10^5 \sin(\pi x) \cos(3\pi y), \quad \beta^+ = 1 + 0.5 \sin(2\pi x) \cos(4\pi y) \quad (13)$$

or

$$\beta^- = 1 + 0.5 \sin(2\pi x) \cos(4\pi y), \quad \beta^+ = 10^6 + 10^5 \sin(\pi x) \cos(3\pi y). \quad (14)$$

The domain is represented in Fig. 6 (right side). We performed one test with (13) and one test with (14). We list in Tables 3 and 4 the errors of the solution and its gradient in the  $L^1$  and  $L^\infty$  norms, while Fig. 8 shows the related bestfit lines.

## 5.3 Example 3: Convergence factor of the multigrid

In this example we show that the asymptotic convergence factor does not depend on the jump of the coefficient and on the size of the problem. The study we want to carry out about the convergence factor concerns how it is close to the optimal one (see Table 5), i.e. the convergence factor predicted by the Local Fourier Analysis for inner equations.

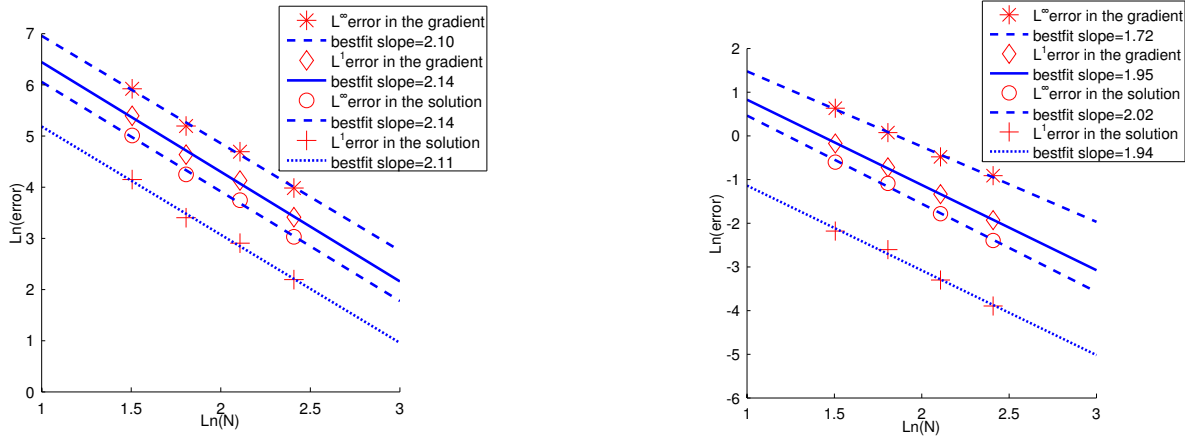


Tab. 3: Example 5.2. Accuracy order in the solution and in the gradient for the case (13).

| $N^2$   | $L^1$ error of $u$ | order | $L^\infty$ error of $u$ | order | $L^1$ error of $ \nabla u $ | order | $L^\infty$ error of $ \nabla u $ | order |
|---------|--------------------|-------|-------------------------|-------|-----------------------------|-------|----------------------------------|-------|
| $32^2$  | $1.41 \cdot 10^4$  | -     | $1.03 \cdot 10^5$       | -     | $2.49 \cdot 10^5$           | -     | $8.38 \cdot 10^5$                | -     |
| $64^2$  | $2.54 \cdot 10^3$  | 2.48  | $1.78 \cdot 10^4$       | 2.53  | $4.34 \cdot 10^4$           | 2.52  | $1.57 \cdot 10^5$                | 2.42  |
| $128^2$ | $8.07 \cdot 10^2$  | 1.65  | $5.58 \cdot 10^3$       | 1.67  | $1.35 \cdot 10^4$           | 1.68  | $4.94 \cdot 10^4$                | 1.67  |
| $256^2$ | $1.57 \cdot 10^2$  | 2.36  | $1.07 \cdot 10^3$       | 2.38  | $2.60 \cdot 10^3$           | 2.38  | $9.65 \cdot 10^3$                | 2.36  |

Tab. 4: Example 5.2. Accuracy order in the solution and in the gradient for the case (14).

| $N^2$   | $L^1$ error of $u$   | order | $L^\infty$ error of $u$ | order | $L^1$ error of $ \nabla u $ | order | $L^\infty$ error of $ \nabla u $ | order |
|---------|----------------------|-------|-------------------------|-------|-----------------------------|-------|----------------------------------|-------|
| $32^2$  | $6.63 \cdot 10^{-3}$ | -     | $2.51 \cdot 10^{-1}$    | -     | $6.70 \cdot 10^{-1}$        | -     | $4.30 \cdot 10^0$                | -     |
| $64^2$  | $2.49 \cdot 10^{-3}$ | 1.41  | $8.18 \cdot 10^{-2}$    | 1.62  | $1.91 \cdot 10^{-1}$        | 1.81  | $1.19 \cdot 10^0$                | 1.86  |
| $128^2$ | $5.02 \cdot 10^{-4}$ | 2.31  | $1.66 \cdot 10^{-2}$    | 2.30  | $4.64 \cdot 10^{-2}$        | 2.04  | $3.31 \cdot 10^{-1}$             | 1.84  |
| $256^2$ | $1.28 \cdot 10^{-4}$ | 1.98  | $4.03 \cdot 10^{-3}$    | 2.04  | $1.18 \cdot 10^{-2}$        | 1.97  | $1.23 \cdot 10^{-1}$             | 1.43  |

Fig. 8: Example 5.2. Bestfit lines of the errors in the solution and in the gradient (Tables 3 and 4) in both the  $L^1$  and  $L^\infty$  norms. Left:  $\beta^-$  and  $\beta^+$  are given by (13); Right:  $\beta^-$  and  $\beta^+$  are given by (13).Tab. 5: Predicted convergence factor  $\rho_{loc}$  by LFA for GS-LEX and FW restriction operator.

| $\nu = \nu_1 + \nu_2$ | 1     | 2     | 3     | 4     |
|-----------------------|-------|-------|-------|-------|
| $\rho_{loc}$          | 0.400 | 0.193 | 0.119 | 0.084 |

Let us recall that we estimate the asymptotic convergence factor as:  $\rho = \lim_{m \rightarrow \infty} \rho^{(m)} = \lim_{m \rightarrow \infty} \left( \frac{\|\mathbf{r}_h^{(m)}\|_\infty}{\|\mathbf{r}_h^{(m-1)}\|_\infty} \right)$ . We perform the homogeneous model problem, namely the Model Problem 1 (1) with  $f^\pm = g_D = g_N = g = 0$  (starting with an initial guess different from zero), in order to avoid difficulties related to numerical instability related to the machine precision.

The numerical tests have been performed by a  $W$ -cycle algorithm with  $\nu_1 = 2$  pre-smoothing and  $\nu_2 = 1$  post-smoothing (therefore  $\nu = 3$  in Table 5), and with the coarsest grid having  $16 \times 16$  grid points. Table 6 shows the

estimated convergence factors in the more complicated geometry of Example 5.2. We choose  $\beta^- = 10^p$ ,  $\beta^+ = 1$ . As we see the convergence factor is quite good over an extremely large range of jumps in the coefficients.

Tab. 6: Example 5.3. Asymptotic convergence factor ( $\nu = \nu_1 + \nu_2 = 3$ ).

| $N^2$   | $p$ | -9     | -7     | -5     | -3     | -1     | 1      | 3      | 5      | 7      | 9      |
|---------|-----|--------|--------|--------|--------|--------|--------|--------|--------|--------|--------|
| $32^2$  |     | 0.0776 | 0.0776 | 0.0776 | 0.0773 | 0.0486 | 0.1563 | 0.1586 | 0.1585 | 0.1585 | 0.1585 |
| $64^2$  |     | 0.0930 | 0.0930 | 0.0930 | 0.0930 | 0.1107 | 0.0931 | 0.1027 | 0.1029 | 0.1029 | 0.1029 |
| $128^2$ |     | 0.1544 | 0.1544 | 0.1544 | 0.1544 | 0.1544 | 0.1543 | 0.1543 | 0.1544 | 0.1544 | 0.1544 |

## References

- [1] L. Adams and Z. Li. The immersed interface/multigrid methods for interface problems. *Journal of Scientific Computing*, 24:463–479, 2002.
- [2] R. E. Alcouffe, A. Brandt, J. Dendy, J. E., and J. W. Painter. The multigrid method for the diffusion equation with strongly discontinuous coefficients. *Journal on Scientific and Statistical Computing*, 2:430–454, 1981.
- [3] A. Coco and G. Russo. Finite-Difference Ghost-Point Multigrid Methods on Cartesian Grids for Elliptic Problems in Arbitrary Domains. *Journal of Computational Physics*. Accepted.
- [4] A. Coco and G. Russo. Second order multigrid methods for elliptic problems with discontinuous coefficients on an arbitrary interface, I: one dimensional problems. *Numerical Mathematics: Theory, Methods and Applications*, 5:19–42, 2012.
- [5] J. J. E. Dendy. Black Box Multigrid. *Journal of Computational Physics*, 48:366–386, 1982.
- [6] R. Mittal and G. Iaccarino. Immersed Boundary Methods. *Annu. Rev. Fluid Mech.*, 37:239–261, 2005.
- [7] J. W. Ruge and Stüben. *Multigrid methods*, chapter Algebraic multigrid, pages 73–130. SIAM, Philadelphia, 1987.
- [8] G. Russo and P. Smereka. A remark on computing distance functions. *Journal of Computational Physics*, 163:51–67, 2000.
- [9] U. Trottemberg, C. Oosterlee, and A. Schuller. *Multigrid*. Academic Press, 2000.
- [10] J. W. L. Wan and X.-D. Liu. A boundary condition-capturing multigrid approach to irregular boundary problems. *Journal of Scientific Computing*, 25:1982–2003, 2004.
- [11] W. L. Wan. Interface preserving coarsening multigrid for elliptic problems with highly discontinuous coefficients. *Numer. Linear Algebra Appl.*, 7:727–741, 2000.